Journal of
Materials Chemistry B

Accepted Manuscript

ROYAL SOCIETY OF CHEMISTRY

www.rsc.org/materialsB

Journal of
Materials Chemistry B

PAPER

Lipid-micelles packaged with semiconducting polymer dots as simultaneous MRI / photoacoustic imaging and photodynamic / photothermal dual-modal therapeutic agents for liver cancer

Received 00th January 20xx,
Accepted 00th January 20xx

DOI: 10.1039/x0xx00000x

www.rsc.org/

Da Zhang[a,b], Ming Wu[a,b], Yongyi Zeng[a,c], Naishun Liao[a,b], Zhixiong Cai[a,b], Gang Liu[d], Xiaolong Liu[a,b,*], Jingfeng Liu[a,b,*]

Incorporating of multiple imaging modality and simultaneous therapeutic functions together into one single nano-formulation is of great importance for developing high performance clinical translatable theranostic agents. Herein, we fabricated multi-functional lipid-micelles incorporated with the semiconducting polymer dots and photosensitizer (referred as Pdots/Ce6@lipid-Gd-DOTA micelles) for combined magnetic resonance imaging (MRI) / photoacoustic imaging (PAI) and photodynamic (PDT) / photothermal (PTT) dual-modal therapy induced by a single laser to achieve enhanced cancer therapeutic efficiency. The Pdots/Ce6@lipid-Gd-DOTA micelles with excellent water dispersibility are comprised of a core with Poly[2,6-(4,4-bis-(2-ethylhexyl)-4H-cyclopenta[2,1-b;3,4-b']-dithiophene)-alt-4,7-(2,1,3-benzo-thiadiazole)]] dots (Pdots) and Ce6 molecules inside, and a lipid-PEG outlayer conjugated with gadolinium-1,4,7,10-tetraacetic acid. The prepared Pdots/Ce6@lipid-Gd-DOTA micelles exhibited extremely low cytotoxicity, and have excellent MR- and PA-imaging contrast enhancement ability, which could synchronous offer anatomical information and morphological information of tumors. Meanwhile, both Pdots and Ce6 photosensitizer, encapsulated into the lipid-Gd-DOTA micelles, with high NIR absorption at 670 nm were applied to combine the photothermal and photodynamic therapy simultaneously to achieve enhanced synergistic cancer therapeutic efficiency both in *vitro* and in *vivo*. In summary, our studies demonstrated that the Pdots/Ce6@lipid-Gd-DOTA micelles with the multi-diagnosis modalities and simultaneous dual-modal photo-therapy functions might be a potential interesting theranostic platform for tumor treatment.

1. Introduction

Photo-therapy is a non-invasive therapeutic technique with many advantages such as remote controllability, improved selectivity, and low systemic toxicity [1]. Photothermal therapy (PTT), which is based on the converting of electromagnetic wave energy to local hyperthermia by photo-absorbing agents has been reported to be an efficient treatment approach to destroy malignant carcinomas under the laser irradiation[2]; photodynamic therapy (PDT), which can transform endogenous oxygen to generate reactive oxygen species (ROS) by photosensitizer to induce the cancer cells apoptosis upon appropriate laser irradiation, has also been clinical applied to treat different tumors [3]. The photosensitizers and photoabsoring agents, which could be activied by near infrared (NIR) laser (650-900 nm), have attracted intensitive interests recently [3-5]. However, several types of photoseneitizers or photoabsorbing agents such as indocyanine green [6] and carbon-based [7, 8] or gold-based [9, 10] materials have its own limitation such as photobleaching, self-destruction, poorly bio-metabolized and the ion-induced toxicity [11]. Moreover, most photosenitizers are inclined to rapidly over-consumption of tissue oxygen that caused severe local hypoxia to stop the production of $^1O_2$ upon laser irradiation [12-14]. Those limitations thus hindered the therapeutic efficacy and restricted further clinical applications [13].

Recently, researchers have found that combination of PDT and PTT together was an effective strategy for enhanced cancer therapy, which could significantly reduce the limitation of each therapeutic modality [15-18]. Unfortunately, due to the absorption mismatch of photosensitizers and photo-absorbing agents at NIR region, most studies have to use different lasers to induce PDT and PTT separately. To simplify this complicated treatment procedure, Chen's groups established a new photosensitizer-loaded gold nano-carrier system for cancer imaging and PDT / PTT treatment using a single laser irradiation [19, 20]. Although gold-based theranostic platform which intrinsi-

[a] The United Innovation of Mengchao Hepatobiliary Technology Key Laboratory of Fujian Province, Mengchao Hepatobiliary Hospital of Fujian Medical University, Fuzhou 350025, P.R. China.
[b] The Liver Center of Fujian Province, Fujian Medical University, Fuzhou 350025, P.R. China.
[c] Liver Disease Center, The First Affiliated Hospital of Fujian Medical University, Fuzhou 350007, P.R. China.
[d] Center for Molecular Imaging and Translational Medicine, Xiamen University.
*Corresponding authors - xiaoloong.liu@gmail.com or drjingfeng@126.com

† Electronic supplementary information (ESI) available: Supporting figures. See DOI: 10.1039/x0xx00000x

cally had both diagnostic imaging ability and therapeutic capability has attracted much attention recently, the clinical usage of these agents is still hindered by the shortages such as sophisticated synthetic process and the heavy metal ion-induced long-term toxicity [9, 21-23]. Compared to the inorganic nanomaterials, the organic-based nanoparticles (lipid/liposome-based nanoparticles such as polymeric micelles of liposomal doxorubicin (Doxil) [24], albumin-bound paclitaxel nanomicelles [25, 26]) have been approved or are currently in clinical trials for the treatment of human cancers. In addition, lipid/liposome-based nanocarriers with the excellent biocompatibility and loading capacity have been developed for delivering photosensitizer and photo-absorbing agents [27-31]. Both PTT and PDT require a precise irradiation region confined to the tumor site, to minimize the side effects. Therefore, the exact information of tumor such as location, distribution, size, shape, boundary, even the biological environment, must be identified before treatment by various imaging tools.

Magnetic resonance imaging (MRI) is one of the most powerful diagnostic imaging tool due to its capability of providing whole-body diffusion-weighted imaging data and timely feedback information of disease tissue, especially in soft tissues [32, 33]. However, unenhanced MRI has the drawbacks of low contrast resolution and sensitivity, which is not enough to provide precise information at the boundary of lesions [34]; while the contrast-enhanced MRI could further provide more detailed anatomical information with high quality and sensitivity [35]. T_1 contrast agents of Gd^{3+}complexes have been predominantly used in clinical MR imaging due to their high contrast enhancing capability without disruption of magnetic homogeneity [36]. However, MRI has certain limitations, such as relatively slow imaging speed, high cost, and inconvenience for general intra-operative usage. Comparing with MRI, photoacoustic imaging (PAI) is a novel optical imaging method, which is based on the measurement of ultrasonic waves generated by the targets with the absorption of short laser pulses, to probe the structure details, functional changes, and molecular states of biological specimens[37, 38]. In combination of the spectral selectivity of laser and the deep spatial penetration of ultrasound, PAI could visualize the lesions at unprecedented depth with high contrast resolution and sensitivity.

Considering that each imaging modality possesses its own characteristic advantages and weaknesses, multi-modal imaging has recently drawn extensive attention in biomedical research due to its ability to provide more comprehensive information for accurate diagnosis. As for the combination of MRI and PAI, MRI can rapidly scan to identify potential lesion locations while PAI can provide information such as high-resolution morphological structure and quantitative information of vulnerable plaque inflammation.

Poly[2,6-(4,4-bis-(2-ethylhexyl)-4H-cyclopenta[2,1-b;3,4-b']-dithiophene)-alt-4,7-(2,1,3-benzo-thiadiazole)]] (PCPDTBT) is a semiconducting π-conjunction polymers that has been widly utilized as a electron donor for polymer:fullerence solar cells [39]. Recently, it has also been used in bio-medical applications because it is completely organic without heavy metal ion-induced toxicities; Rao's group has fabricated a PCPDTBT nanohybrid (SPN1) with excellent photo-acoustic effect for in vivo photoacoustic molecular imaging [40]. Interestingly, we discovered that the PCPDTBT nano dots also exhibited an excellent NIR aborption with the peak at 670 nm; the strong NIR aborption of Pdots might be utilized as a potential new photo-absorbing agent for photothermal therapy. Previously, we have reported the polydopamine (PDA) nanoparticles conjugated with Chlorin e6 as dual-modal therapeutic agents for enhanced cancer therapy through two seperated laser irradiation (670 nm and 808 nm) [16]. Herein, we fabricated photosensitizer (Ce6) and PCPDTBT dots (Pdots) co-loaded lipid-micelles, which is constructed from the self-assemble of gadolinium-1,4,7,10-tetraacetic acid modified phospholipid-PEG lipids (refered as lipid-Gd-DOTA micelles), for the MRI/PAI dual-modal cancer imaging and the simultaneously combined PDT/PTT therapy through a single laser irradiation.

2. Experimental

2.1. Materials

Poly[2,6-(4,4-bis-(2-ethylhexyl)-4H-cyclopenta[2,1-b;3,4-b']-dithiophene)-alt-4,7-(2,1,3-benzothiadiazole)] (PCPDTBT), Chlorin e6 (Ce6), N-(3-Dimethylamino-propyl)-N-ethylcarbodiimide hydrochloride (EDC), N-hydroxysuccinimide (NHS), 9, 10-anthracenediylbis (methylene) dimalonic acid (ABDA) and 2', 7'-dichlorodihydrofluorescein diacetate (DCFH-DA) were purchased from Sigma-Aldrich. The molecular weight of PCPDTBT is 7,000~20,000 (Mw). The 2-distearoyl-sn-glycero-3-phosphoethanolamine-N-[amino(polyethylene glycol)-2000] (H_2N-PEG-DSPE) and 1-palmitoyl-2-stearoyl-sn-glycero-3-phosphatidylcholine (HSPC) were purchased from Nanocs. The 1, 4, 7, 10-tetraacetic acid mono-N-hydroxysuccinimide ester (DOTA-NHS) was purchased from Macrocyclics. The LIVE/DEAD Viability/Cytotoxicity Kit was purchased from Invitrogen (Eugene, OR, USA). Annexin V-fluoroisothio cyanate (FITC))/propidium iodide (PI) apoptosis detection kit and Cell Counting Kit-8 (CCK8) were purchased from Dojindo Laboratories. Deionized water with a resistivity of 18.2 MΩ•cm was obtained from a Milli-Q Gradient System (Millipore, Bedford, MA, USA) and used for all experiments. Unless specified, all other chemicals were commercially available and used as received.

2.2. Cell culture

The human hepatocellular carcinoma cancer cell line HepG2, and the NIH-3T3 fibroblast cells were maintained as monolayer cultures in RPMI-1640 medium supplemented with 10% fetal bovine serum (FBS, Atlanta Biologicals, Lawrenceville, GA, USA) and 1% penicillin-streptomycin (Gibco BRL, Grand Island, NY, USA) at 37ºC in a humidity atmosphere (5% CO_2).

2.3. Synthesis of the Pdots/Ce6@lipid-Gd-DOTA micelles

Pdots/Ce6@lipid-Gd-DOTA micelles were prepared by matrix-enacapsulation method [41]. First, lipid-DOTA (DSPE-PEG-DOTA) was prepared by our previously reported method through the amide reaction of the -NH_2 terminal group of DSPE-PEG with the -NHS group of DOTA-NHS [42]. After-

wards, the prepared lipid-DOTA was mixed with the $GdCl_3$ to obtain the lipid-Gd-DOTA (DSPE-PEG-DOTA-Gd) through chelation the Gd (III). The ^{1}H NMR of lipid-Gd-DOTA was perfomed to demonstrate the successful coupling of DOTA-NHS and DSPE-PEG. As shown in Figure S1, the peaks assigned to lipid-PEG (δ 3.64, 1.25, and 0.88 ppm) and DOTA-NHS (δ 1.59, 1.25, and 0.83 ppm) were present in the ^{1}H NMR of the lipid-Gd-DOTA (DSPE-PEG-DOTA-Gd). Subsequently, 1 mL of the tetrahydrofuran mixture solution that contained PCPDTBT (0.25 mg), Chlorin e6 (Ce6) (0.5 mg), HSPC (2.5 mg), and lipid-Gd-DOTA (0.5 mg), were rapidly injected into 10 mL Milli-Q water, then followed by sonication for 1.5 min at 40 W output using a microtip probe sonicator. The mixture was then stirred at 600 rpm/min at room temperature in dark overnight for evaporation of tetrahydrofuran solution. The suspension of formed nanomicelles was then dialyzed against deionized water for 48h (MWCO = 14000 Da) to remove excess Ce6, and PCPDTBT dots. Subsequently, the obtained products (Pdots/Ce6@lipid-Gd-DOTA micelles) were resuspended in Milli-Q water, and the concentration was adjusted from 0.1 mg/mL (Pdots, 16 μg/mL; Ce6, 24 μg/mL) to 1 mg/mL (Pdots, 160 μg/mL; Ce6, 240 μg/mL). The amount of loaded Ce6 or PCPDTBT dots were determined by measuring the absorbance at 405 nm in DMSO or 698 nm in THF, respectively. The amount of Gd was determined through XSERIES 2 inductively coupled plasma mass spectrometry (ICP-MS) (Thermo, USA). To serve as a control, an analogous micelles, but without Ce6 and Gd-DOTA (referred as Pdots@lipid micelles), were also prepared. The synthesis procedure of the Pdots@lipid micelles was similar to that of Pdots/Ce6@lipid-Gd-DOTA micelles, with replacing the lipid-Gd-DOTA by lipid-PEG, and without loading Ce6. In addition, other micelles without Gd-DOTA (referred as Pdots/Ce6@lipid micelles) were also prepared. The synthesis procedure of Pdots/Ce6@lipid micelles was also similar to that of Pdots/Ce6@lipid-Gd-DOTA micelles, but the lipid-Gd-DOTA was replaced by lipid-PEG.

2.4. Characterization of the Pdots/Ce6@lipid-Gd-DOTA micelles

TEM was performed by using a JEM-2010 electron microscope (JEOL, Japan) to characterize the overall morphology and the chemical compositions of the nanomicelles. DLS experiments were performed at 25ºC on a Nano ZS (Malvern Instruments, Malvern UK) with a detection angle of 173° and a 3-mW He-Ne laser operating at the wavelength of 633 nm; briefly, 1 mL dispersion of Pdots/Ce6@lipid-Gd-DOTA micelles (0.05 mg/mL) was placed into a glass cuvette, and then the sample was measured; the average value was obtained from 3 replicated measurements for each sample; the PDI values were obtained by analyzing the correlation functions through cumulants analysis. Zeta potential measurements were performed at 25°C on the NanoZS using the M3-PALS technology. FT-IR spectrum of the prepared Pdots/Ce6@lipid-Gd-DOTA micelles was collected on a FT-IR spectrometer (Perkin Elmer, USA); briefly the samples were mixed with KBr, compressed to a plate, and evaluated over the spectral region of 400 to 4000 cm^{-1}. The UV-NIR absorption spectra of the Pdots/Ce6@lipid-Gd-DOTA micelles were measured by a Vis-NIR spectrometer (Spectro Max M5e, Germany).

2.5. Temperature elevation and ROS generation under 670 nm laser irradiation

To study the photothermal effect of Pdots/Ce6@lipid-Gd-DOTA micelles, 2 mL aqueous solution of the lipid-micelles was irradiated by a 670 nm laser with the power density of 0.5 W/cm^2. The temperature of the solution was monitored by a thermocouple microprobe (Φ = 0.5 mm) (STPC-510P, Xiamen Baidewo Technology Co., China) that was submerged in the solution every 10s. ROS generation of the Pdots/Ce6@lipid-Gd-DOTA micelles was measured through using ABDA as an indicator. Briefly, the Pdots/Ce6@lipid-Gd-DOTA micelles (Ce6: 24 μg/mL) in Milli-Q water containing 20 mM ABDA was irradiated by a 670 nm laser with the power intensity of 0.5 W/cm2 for 0, 1, 3, 5, 7, 9 and 11 min, respectively; afterwards, the absorbance change of ABDA from 300 to 450 nm was measured by a UV-Vis spectrometer (Spectro Max M5e, Germany).

2.6. In vitro cellular uptake measurment by flow cytometry

HepG2 cells were seeded into 6 well plates at a density of 1×10^6 cells per well, and incubated in a humidity atmosphere with 5% CO_2 for 24 h. Then the original medium was replaced with fresh culture medium containing 0.05 mg/mL Pdots/Ce6@lipid-Gd-DOTA micelles (Pdots, 8 μg/mL; Ce6, 12 μg/mL). After incubating for 1, 2, 3 and 4h, the cells were washed three times with PBS solution, and then dispersed in 1 mL PBS. Afterwards, the cells were filtered through a 40 microns nylon mesh to remove cell aggregates before fluorescence-activated cell sorting (FACS) analysis. Fluorescence measurement of the intracellular Ce6 was done in the FL4 channel with the excitation at 670 nm [16].

2.7. Confocal microscopy studies of the cellular uptake of Pdots/Ce6@lipid-Gd-DOTA micelles

The uptake of Pdots/Ce6@lipid-Gd-DOTA micelles by HepG2 cells was investigated by confocal microscopy. HepG2 cells (5×10^4) were seeded into 35-mm glass-bottom Petri dishes and cultured for 24 h at 37°C in the incubator. Then, the Pdots/Ce6@lipid-Gd-DOTA micelles were added to the cells and further incubated for 3 h. After that, Propidium iodide (PI) was added into the Petri dishes and then incubated in the dark for 15 min at room temperature. Subsequently, the HepG2 cells were washed three times with PBS (pH 7.4) at room temperature and then fixed with 4% paraformaldehyde for 15 min. Finally, the cells were imaged by a confocal microscope (LSM 780, USA) with 543 nm laser excitation for Ce6.

2.8. In vitro cytotoxicity analysis and photodynamic / photothermal ablation of cancer cells

The cytotoxicity of Pdots/Ce6@lipid-Gd-DOTA micelles was evaluated on HepG2 cells and NIH-3T3 fibroblast cells using Cell Counting Kit (CCK8). The cells were seeded in a 96-well plate at a density of 1×10^5 cells per well and incubated in a humidity atmosphere (with 5% CO_2) for 24 h. Then, the original medium was replaced with fresh culture medium containing

Pdots/Ce6@lipid-Gd-DOTA micelles at a final Pdots concentration ranging from 1 to 16 μg/mL. Meanwhile, the cells incubated with cell culture medium only were prepared as untreated control. The medium was aspirated after 48 h incubation, and the cells were washed twice with 100 μL PBS solution. Subsequently, 100 μL of culture medium and 10 μL of CCK8 solution were added to the wells. After incubation for 2 h at 37 °C, the absorbance of the solution in each well at 450 nm was measured with a microplate reader (Spectra Max M5e, Germany). The proliferation of cells was determined by the absorption intensity. Cell viability was expressed as follows: Cell viability (%) = (OD sample-OD blank) / (OD control-OD blank) × 100%. The OD sample and OD control are the absorbance values of the treated cells (as indicated) and the untreated control cells (without nanoparticles), respectively. The OD blank was the absorbance of CCK8 reagent itself at 450 nm. All experiments were performed in quadruplicate.

To investigate the photo killing efficiency of Pdots/Ce6@lipid-Gd-DOTA micelles, HepG2 cells were first seeded into a 96-well plate at a density of 1×10^5 cells per well at 37°C in a 5% CO_2 atmosphere for 24 h. Then, the cells were washed three times with PBS to remove dead cells, followed by incubation with different concentrations of Pdots/Ce6@lipid-Gd-DOTA micelles, Pdots@lipid micelles and Ce6 dispersed in RPMI-1640 medium at 37°C for 3 h. Next, the cells were washed three times with PBS buffer. Then, the cells were exposed to 670 nm laser (0.5 W/cm^2) for 5 min. After laser irradiation, the cells were incubated with fresh RPMI-1640 culture medium containing 10% fetal bovine serum at 37°C for 24 h. Then, the cell viability was determined by CCK8 according to the above mentioned procedure.

Localized photo-killing effects of the Pdots/Ce6@lipid-Gd-DOTA micelles were also evaluated on HepG2 cells as follows. HepG2 cells were first seeded into a 6-well plate at a density of 1×10^6 cells per well at 37°C in a 5% CO_2 atmosphere for 24 h. Then, the cells were washed three times with PBS to remove dead cells, followed by incubation with Pdots/Ce6@lipid-Gd-DOTA micelles, Pdots @lipid micelles or Ce6 (all at the Ce6 concerntration of 2.4 μg/mL) dispersed in culture medium at 37°C for 3 h. Afterwards, the cells were washed by PBS buffer to remove none uptaken micelles, and then exposed to 670 nm laser (0.5 W/cm^2) for 5 min, respectively. After laser irradiation, the cells were incubated with fresh culture medium at 37°C for 2 h. Then, the cells were stained with LIVE/DEAD Viability/Cytotoxicity Kit for the visualization of live and dead cells. Next, we used Annexin-V-FITC / propidium iodide (PI) staining method to further evaluate cell apoptosis induced by the photothermal / photodynamic treatment of Pdots/Ce6@lipid-Gd-DOTA micelles. Briefly, HepG2 cells were first seeded into a 6-well plate at a density of 1×10^6 cells per well at 37°C in a 5% CO_2 atmosphere for 24 h. Then, the cells were washed three times with PBS to remove dead cells, followed by incubation with Pdots/Ce6@lipid-Gd-DOTA micelles, Pdots @lipid micelles and Ce6 (Ce6, 2.4 μg/mL) dispersed in culture medium at 37°C for 3 h. Next, the cells were washed by PBS buffer to remove none uptaken micelles, and then exposed to 670 nm laser (0.5 W/cm^2) for 5 min, respectively. After laser irradiation, the cells were incubated with fresh culture medium at 37°C for 24 h. Then, the cells were collected and resuspended in 500 μL of binding buffer, and Annexin V-FITC and Propidium iodide (PI) were added following the manufacturer's recommendation. Samples were incubated in the dark for 15 min at room temperature and then analyzed using flow cytometry.

2.9. In Vitro and in Vivo MRI Measurement

Aqueous dispersions of the Pdots/Ce6@lipid-Gd-DOTA micelles at different concentration were investigated using T_1/T_2 -weighted MRI on a 9.4 T small animal MRI scanner (Bruker Avance II 500 WB spectrometer) to evaluate the contrast-enhancement effect. T_1/T_2-weighted imaging was performed using an inversion recovery gradient echo sequence with TE = 4 ms, a slice thickness of 0.5 mm, an field of view (FOV) of 3.0 × 3.0 cm, and a matrix size of 128 × 128. Injected dimeglumine gadopentetate (a commercial MRI contrast agent) was used as a control. MRI imaging data of tumor site were collected before and after 2 h of the intratumoral injection of Pdots/Ce6@lipid-Gd-DOTA micelles (100 μL, 0.1 mg/mL).

2.10. In Vitro and In Vivo Photoacoustic Imaging

In vivo PA imaging was carried out on HepG2 tumor-bearing nude mice (22-24 g). The photoacoustic signals were excited by using a Q-switched Nd:YAG laser (LS-2137/2, LOTIS TII, Minsk, Belarus) and a pumped tunable Ti: sapphire laser (LT-45 2211A, LOTIS TII, Minsk, Belarus). An unfocused ultrasonic transducer with a central frequency of 2.25 MHz was used to detect the photoacoustic signals at 680 nm. Before imaging, the mouse was first anesthetized and placed on a homemade shelf. Afterwards, a thin layer of ultrasonic coupling gel was coated on the tumor, and then the tumor was placed on the bulge at the tank's bottom and the bulge site was immersed in water. PA imaging data of tumor site was collected before and after the intratumoral injection of Pdots/Ce6@lipid-Gd-DOTA micelles (100 μL, 0.1 mg/mL).

2.11. Tumor xenograft and in vivo photodynamic / photothermal therapy

Immunodeficiecy male nude mice with a body weight of ~26 g from China Wushi, Inc. (Shanghai, China) were used for the animal study. All animal procedures were approved by the Animal Ethics Committee of Fujian Medical University. Tumor-bearing nude mice were prepared by subcutaneously injecting a suspension of the HepG2 cells (107 cells) in sterilized 1× PBS. When the tumor size reached 130~170 mm^3, 0.1 mg/mL of the Pdots/Ce6@lipid-Gd-DOTA micelles (with Pdots concerntration of 16 μg/mL, or Ce6 concerntration of 24 μg/mL; 50 μL injection of each mouse) were intratumoral injected into each mouse (n=5). One group of mice treated with the same volume of sterilized PBS was taken as control. The mice were segregated into 4 groups: (1) PBS-treated groups with 670 nm (0.5 W/cm^2) laser irradiation for 10 min (n=5); (2) Ce6-treated groups with 670 nm (0.5 W/cm^2) laser irradiation for 10 min (n=5); (3) Pdots@lipid-treated groups with 670 nm (0.5 W/cm^2) laser irradiation for 10 min (n=5); (4) Pdots/Ce6@lipid-Gd-

DOTA-treated with 670 nm (0.5 W/cm^2) laser irradiation for 10 min (n=5). The irradiation was conducted after 2h of injection. The therapeutic effects were evaluated by monitoring the tumor volume and body weight changes in each group every two days up to 19 days. The size of tumors was measured by caliper every other day after the treatment. The volume of tumor (V) was calculated by the following equation: $V = A \times B^2 / 2$, where A and B are the longer and shorter diameter (mm) of the tumors respectively.

2.12. Histological examination and long-term toxicity assessment

To examine the histological changes of the tumors, one tumor-bearing mouse in each group was sacrificed after 24h of laser irradiation, and the tumors were collected, and then stained with Hematoxylin and eosin (H&E) for histopathology evaluation and Ki67 antibody for immunohistochemical analysis. To assess the long-term systematic toxicities of Pdots/Ce6@lipid-Gd-DOTA micelles, the lipid-micelles treated Balb/c mice were sacrificed at the time point of 0, 1, 8, 20 days after intravenous injection of Pdots/Ce6@lipid-Gd-DOTA micelles (Pdots, 16 μg/mL; Ce6, 24 μg/mL; 100 μL injection of each mouse) via tail vein, and the major organs (heart, liver, spleen, lungs and kidney) of those mice were then collected, fixed in 4% neutral formaldehyde, conducted with paraffin embedded sections, stained with hematoxylin and eosin, and observed under a Zeiss microscope (Axio Lab.A1).

Results and discussion

3.1. Synthesis and Characterization of Pdots/Ce6@lipid-Gd-DOTA micelles

In this work, Pdots/Ce6@lipid-Gd-DOTA micelles were prepared by the matrix-enacapsulation method [41] (Figure 1 A). Firstly, the gadolinium-1,4,7,10-tetraacetic acid (Gd-DOTA) was conjugated with [polyethylene glycol-2000]-2-distearoyl-sn-glycero-3- phosphoethanolamine (lipid-PEG) to obtain lipid-Gd-DOTA as a MRI contrast agent according to our pervious works [42]. Secondly, the lipid-Gd-DOTA was added into the THF solution that contained semiconducting polymers of poly[2,6-(4,4-bis-(2-ethylhexyl)-4H-cyclopenta[2,1-b;3,4-b']-dithiophene)-alt-4,7-(2,1,3-benzothiadiazole)] (PCPDTBT), Chlorin e6 (Ce6) and 1-palmitoyl-2-stearoyl-sn-glycero-3-phosphatidylcholine (HSPC) (at a mass ratio of 2:1:2:5). Afterwards, the mixture was rapidly injected into water, and then followed by sonication. The semiconducting polymer of PCPDTBT dots (Pdots) and Ce6 molecules were co-loaded into the lipid-Gd-DOTA micelles via π-π stacking and hydrophobic interaction. The drug loading efficiency of Pdots and Ce6 in the micelles were 16 wt% and 24 wt% respectively, which was determined by the absorbance of PCPDTBT in THF at 698 nm and Ce6 in DMSO at 405 nm (Figure S2) respectively. To verify the successful synthesis of Pdots/Ce6@lipid-Gd-DOTA micelles, Vis-NIR spectra of free Ce6 in DMSO, Pdots@lipid micelles and Pdots/Ce6@lipid-Gd-DOTA micelles were obtained, as shown in Figure 1B. Compared with the absorbance of Pdots@lipid micelles (red lines), Pdots/Ce6@lipid-Gd-DOTA micelles (black lines) exhibited higher absorption peaks at 405 nm (Soret peak) and 675 nm (Q-band), corresponding to the characteristic absorption peak of free Ce6 (green lines), indicated the successful loading of Ce6 molecules. Transmission electron microscopy (TEM) images showed the Pdots/Ce6@lipid-Gd-DOTA micelles could be well dispersed in aqueous solution, demonstrating an average diameter of 36 ± 8 nm (Figure 1C). The enlarged photography provided the details that the amount of punctate pattern of Pdots (black dot) with sizes of 3~4 nm were uniformly distributed in the interior of the micelles (Figure 1D and Figure S3). Dynamic light scattering (DLS) studies showed that the average hydrodynamic size of Pdots/Ce6@lipid-Gd-DOTA micelles was 111.5 ± 3.16 nm (Figure 2A). The PDI of Pdots/Ce6@lipid-Gd-DOTA micelles is determined to be 0.289 by DLS, indicating a relatively narrow size distribution. The larger size of Pdots/Ce6@lipid-Gd-DOTA micelles determined by DLS than the size determined by TEM is mainly attributed to the slightly aggregation of this micelles in water.

To further investigate the influence of lipid-Gd-DOTA on zeta potential of the Pdots/Ce6@lipid-Gd-DOTA micelles, Pdots/Ce6@lipid micelles without Gd-DOTA were synthesized as the same as above described procedure (as detail mentioned in the Experimental Section). As shown in Figure 2B, Pdots@lipid micelles without Ce6 molecules loaded exhibited a negative surface charge (-17.16 ± 1.4 mV) in aqueous solution at pH 7.4, which ascribed to phosphate anion in the polar head of HSPC. After loading Ce6, the zeta potential of Pdots/Ce6@lipid micelles (ζ) turned to -38.8 ± 4.2 mV. However, its zeta potential was switched to 2.9 ± 0.7 mV after assembling with the neutral charged lipid-Gd-DOTA, since the chelated Gd (Ⅲ) could neutralize the remained 3 negatively charged COO^- group of lipid-DOTA then the obtained lipid-Gd-DOTA had no charged groups in its hydrophilic heads.

To further verify the existence of Ce6 and Pdots inside the Pdots/Ce6@lipid-Gd-DOTA micelles, fourier transform infrared (FT-IR) spectra of all the components of Pdots/Ce6@lipid-Gd-DOTA micelles, Pdots@lipid micelles, Ce6 and PCPDTBT were obtained. As shown in Figure S4, Pdots/Ce6@lipid-Gd-DOTA micelles presented a specific absorption feature, and the presence of new bands at 1594 cm^{-1} (N-H in-plane) and 1340 cm^{-1} (C–N stretching) confirmed the successful formation of amide groups by chemical conjugation of the surface carboxylic acid groups of the Gd-DOTA with the amine-terminated of the phospholipid-PEG. Meanwhile, the feature bands are including the bands at 3410 cm^{-1} (stretching vibration of phenolic O-H and N-H), 1610 cm^{-1} (stretching vibration of aromatic ring and bending vibration of N-H), 1510 cm^{-1} (shearing vibration of N-H) and 1068 cm-1 (C-O stretching), and those spectrum confirmed the successful loading of PCPDTBT dots and Ce6 photosensitizers (Figure S4).

3.2. Synchronous ROS generation and Temperature Elevation Induced by 670 nm NIR laser irradiation

Previously, we have demonstrated that Pdots and Ce6 photosensitizer showed the high NIR absorption at 670 nm, therefore our prepared lipid-micelles might be a promising PDT / PTT

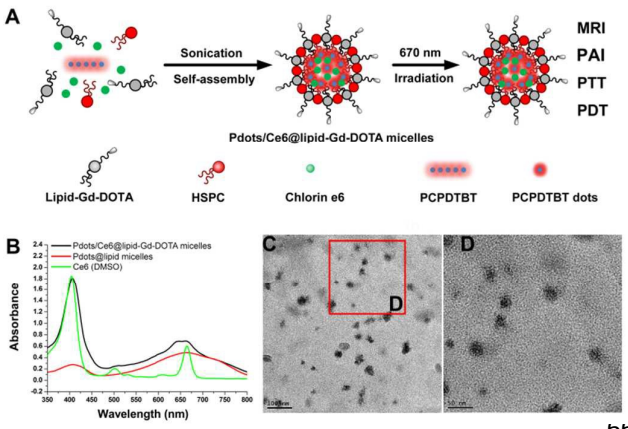

Figure 1. (A) A schematic view of the design of Pdots/Ce6@lipid-Gd-DOTA micelles. (B) The vis-NIR spectra of the Ce6 (in DMSO), as well as Pdots@lipid micelles and Pdots/Ce6@lipid-Gd-DOTA micelles in water. (C) Representative TEM image of the prepared Pdots/Ce6@lipid-Gd-DOTA micelles (scale bar = 100 nm). D) The enlarged images of Pdots/Ce6@lipid-Gd-DOTA micelles (scale bar = 50 nm).

dual-modal therapeutic agent induced by a single laser for cancer therapy. ROS is primarily responsible for the cell death, which is the key parameter to estimate the PDT effect. To investigate the PDT effect, we firstly used 9, 10-anthracenediyl-bis (methylene) dimalonic acid (ABDA) as an indicator to evaluate the ROS production of the Pdots/Ce6@lipid-Gd-DOTA micelles under NIR laser irradiation. As shown in Figure 2C and S5, the Pdots/Ce6@lipid-Gd-DOTA micelles (Pdots 16 μg/mL; Ce6 24 μg/mL) in water and free Ce6 (24 μg/mL) in DMSO exhibited a sharp decline in ABDA absorbance at the range from 300 to 400 nm under 670 nm laser irradiation at the power intensity of 0.5 W/cm^2 for 7 min (the same laser wavelength and intensity was used in all the experiments), while there is no decrease of the absorbance with the equivalent laser power irradiation when only existed ABDA. In addition, to further confirm that the ROS is generated from the loaded Ce6 molecules, we compared the ROS production of Pdots/Ce6@lipid-Gd-DOTA micelles with that of Pdots@lipid micelles (Pdots 16 μg/mL) or free Ce6 (DMSO) (Ce6 24 μg/mL) under 670 nm laser irradiation. As shown in Figure 2D, the Pdots/Ce6@lipid-Gd-DOTA micelles and free Ce6 (DMSO) produced almost the same amount of ROS after exposure to laser for 11 min, but the Pdots@lipid micelles alone could not generate any ROS under the same conditions. These evidence suggested that the ROS was mainly generated from the loaded Ce6 molecules of Pdots/Ce6@lipid-Gd-DOTA micelles. Furthermore, the photothermal conversion of Pdots/Ce6@lipid-Gd-DOTA micelles was also carefully evaluated. As shown in Figure 2E, the temperature of Pdots/Ce6@lipid-Gd-DOTA micelles, which contain 2, 4, 8, 16 μg/mL of Pdots, was increased up to 38.4°C, 43.9°C, 50.6°C and 53.4°C after exposure to laser for 10 min, respectively. At the Pdots concentration of 8 μg/mL, the temperature was already increased up to 50.6°C, which is sufficient to induce the cancer cells necrosis (Figure 2 F). In contrast, the temperature of the De-ion water was not significantly changed (26.4°C) when exposed to laser irradiation. These results indicated that the Pdots inside our lipid-micelles were primarily responsible for the photothermal conversion. Furthermore, the photothermal stability of the photo-absorbing agents during NIR laser irradiation is essential in PTT applications. To investigate the photothermal stability, the Pdots/Ce6@lipid-Gd-DOTA micelles were subjected to four rounds of repeated irradiation using laser on/off cycling as follows: the Pdots/Ce6@lipid-Gd-DOTA micelles were irradiated by NIR laser for 500s (laser on), followed by naturally cooling to room temperature without NIR laser irradiation (laser off). As shown in Figure S6, the Pdots/Ce6@lipid-Gd-DOTA micelles maintained excellent photothermal stability during repeated irradiation without experiencing any decrease in their temperature elevation ability, which suggested that Pdots/Ce6@lipid-Gd-DOTA micelles could act as a stable photothermal conversion agent. In summary, these results clearly indicated that our prepared Pdots/Ce6@lipid-Gd-DOTA micelle could act as an excellent dual-modal photo-therapeutic agent with high ROS generation ability and excellent photothermal conversion ability induced by a single laser irradiation.

3.3. Evaluation of the cellular uptake of Pdots/Ce6@lipid-Gd-DOTA micelles

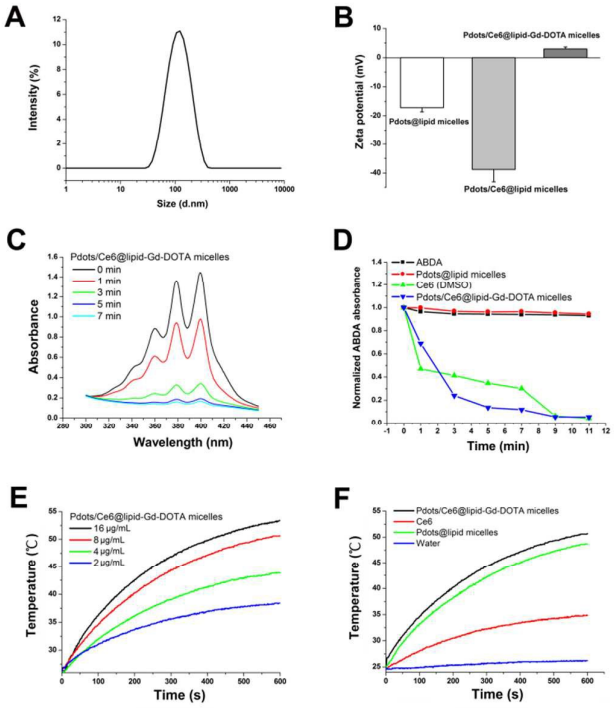

Figure 2. (A) Hydrodynamic size of Pdots/Ce6@lipid-Gd-DOTA micelles in water. (B) The surface zeta potential of the Pdots@lipid micelles, Pdots/Ce6@lipid micelles and Pdots/Ce6@lipid-Gd-DOTA micelles. (C) The absorbance of 9,10-dimethylanthracene (ABDA, 20 mM) after photodecomposition by ROS generation upon 670 nm laser irradiation at 0.5 W/cm^2 in the presence of Pdots/Ce6@lipid-Gd-DOTA micelles in water; (D) Normalized absorbance of 9, 10-imethylanthracene (ABDA, 20 mM) at 380 nm during photodecomposition by ROS generation upon 670 nm laser irradiation at 0.5 W/cm^2 in the presence of PBS solution alone, Pdots@lipid micelles in PBS solution, Ce6 in DMSO and Pdots/Ce6@lipid-Gd-DOTA micelles in PBS solution, respectively. (E) Temperature elevation curves of the Pdots/Ce6@lipid-Gd-DOTA micelles with different concentrations; (F) Temperature elevation curves of DI-water, free Ce6, Pdots@lipid micelles and Pdots/Ce6@lipid-Gd-DOTA micelles at the same concentration of Pdots or Ce6.

Efficient internalization of Pdots/Ce6@lipid-Gd-DOTA micelles by cancer cells were of great importance in cancer therapy. Here, we first used flow cytometry to quantify the internalization efficiency of the Pdots/Ce6@lipid-Gd-DOTA micelles in HepG2 cells after 1, 2, 3 and 4h incubation. As shown in Figure 3A, the Ce6 fluorescence intensities of the Pdots/Ce6@lipid-Gd-DOTA micelles treated HepG2 cells were increased in a time-dependent manner from 1 to 3 h, and remained unchanged after 3h. To further comfirm that the fluorescence signals are coming from the loaded Ce6 photosensitizer, confocal microscopy was conducted. As shown in Figure 3B, the red fluorescence signal from the internalized Pdots/Ce6@lipid-Gd-DOTA micelles in HepG2 cells could be clearly observed. In contrast, the fluorescence signal of Pdots@lipid micelles treated HepG2 was not observed, and the red fluorescence signal of the HepG2 cells incubated with the same concentration of free Ce6 was lower than that of Pdots/Ce6@lipid-Gd-DOTA micelles treated cells. These data demonstrated that the Pdots/Ce6@lipid-Gd-DOTA micelles could be effectively internalized by HepG2 cells.

3.4. In vitro phototoxicity induced cell death

Nontoxicity or low toxicity is a key criterion of any nanomaterials designed for biomedical applications. Cell viability assays (CCK8) were performed to investigate the cytotoxicity of Pdots/Ce6@lipid-Gd-DOTA micelles in the NIH-3T3 cells. As shown in Figure 3C, both of the Pdots/Ce6@lipid-Gd-DOTA micelles and Pdots@lipid micelles showed a very low cytotoxic effect on the NIH-3T3 cells in the absence of laser irradiation, and the cells remained more than 95% viable even when the concentration was increased up to 16 μg/mL (Pdots, Ce6 24 μg/mL) with 48 h incubation.

As above mentioned, we have demonstrated that Pdots/Ce6@lipid-Gd-DOTA micelles could produce significant

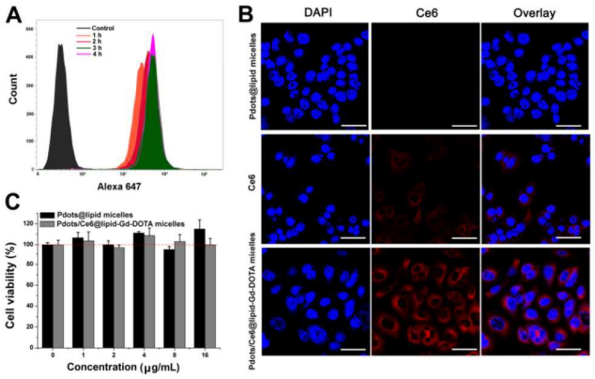

Figure 3. (A) Flow cytometry analysis of Ce6 fluorescence inside the cells after incubation with Pdots/Ce6@lipid-Gd-DOTA micelles for 1, 2, 3 and 4h, respectively. The mean fluorescence intensities (MFI) of Ce6 at different incubation time points were indicated as insert. (B) Confocal images of HepG2 cells incubated with free Ce6, Pdots@lipid micelles and Pdots/Ce6@lipid-Gd-DOTA micelles for 3h, respectively (Scale bar = 50 μm). (C) Cell viability of NIH-3T3 cells treated with different concentration of the Pdots@lipid micelles and Pdots/Ce6@lipid-Gd-DOTA micelles without laser irradiation.

ROS upon the 670 nm laser irradiation in aqueous media, which could subsequently damage the cancer cells by ROS induced cells apoptosis. Then, we examined the intracellular ROS generation by 2', 7'-dichlorodihydrofluorescein diacetate (DCFH-DA) that was widely applied as a ROS fluorescence indicator. As shown in Figure 4A, the untreated control cells showed a low DCFH-DA fluorescence signal, indicating that only a few ROS was present inside the cancer cells. Meanwhile, neither the laser irradiation alone at 670 nm nor the presence of Pdots@lipid micelles with laser irradiation could induce additional ROS production comparing to the control group. In contrast, there was a very strong DCFH-DA fluorescence signal in the cells treated with Pdots/Ce6@lipid-Gd-DOTA micelles under the 670 nm laser irradiation, and it was much higher than that of free Ce6-treated cells due to the efficient cellular uptake of Pdots/Ce6@lipid-Gd-DOTA micelles (Figure 3B). However, without laser irradiation, the Pdots/Ce6@lipid-Gd-DOTA micelles themselves could not produce any additional DCFH-DA fluorescence signal rather than the background. These results

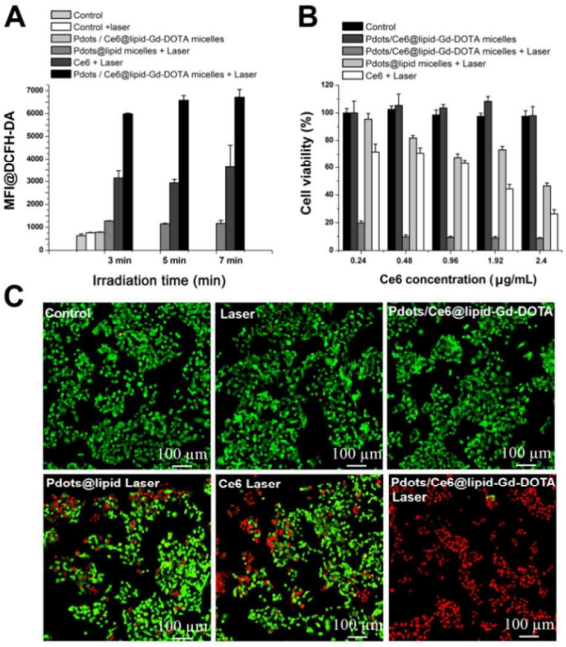

Figure 4. (A) The mean fluorescence intensity of DCFH-DA which represented $^1O_2$ production in each group as indicated: none treated cells as a control; cells with 670 nm laser irradaiton alone; cells with 670 nm laser irradiation in the presence of free Ce6, Pdots@lipid micelles or Pdots/Ce6@lipid-Gd-DOTA micelles, respectively. The 670 nm laser power intensity is 0.5 W/cm^2. (B) Cell viability of HepG2 cells treated with different concentration of free Ce6, Pdots@lipid micelles and Pdots/Ce6@lipid-Gd-DOTA micelles upon 670 nm laser light. Bars, means±SD (n = 6). (C) Fluorescence images of the live/dead viability totoxicity kit stained HepG2 cells in following conditions: HepG2 cells without treatment; HepG2 cells with laser light alone; HepG2 cells incubated with Pdots/Ce6@lipid-Gd-DOTA micelles without laser irradiation; HepG2 cells were irradiated with 670 nm laser in the presence of free Ce6, Pdots@lipid micelles or Pdots/Ce6@lipid-Gd-DOTA micelles, respectively. scale bar = 100 μm.

proved that ROS could be selectively generated in the Pdots/Ce6@lipid-Gd-DOTA micelle treated cells upon 670 nm NIR irradiation, which could be applied as a promising agent for PDT treatment.

Furthermore, the photothermal conversion and ROS generation of our Pdots/Ce6@lipid-Gd-DOTA micelles prompt us to evaluate their feasibility as a PTT / PDT dual-modal therapeutic agent. CCK8 was conducted to evaluate the cell killing efficiency induced by laser irradiation. As shown in Figue 4b, the free Ce6 and Pdots@lipid micelles showed a dose-denpendent PDT effect and PTT effect under 670 nm laser irradiation, and the viability of Ce6 (2.4 μg/mL) or Pdots@lipid micelles (Pdots,1.6 μg/mL) treated HepG2 cells was sharply decreased to 25.6% and 44.7% under 670 nm laser irradiation. While the cell viability of Pdots/Ce6@lipid-Gd-DOTA micelles treated HepG2 cells was further decreased down to 15.3% at the same concentration (Ce6, 2.4 μg/mL; Pdots, 1.6 μg/mL) under 670 nm laser irradiation, which indicated the excellent synergistic killing efficiency to cancer cells. However, the Pdots/Ce6@lipid-Gd-DOTA micelles themselves had no PTT or PDT effect against HepG2 cells without laser irradiation.

To further evaluate the localized photo-killing effect of the synergistic photo-therapy, HepG2 cells were incubated with Pdots/Ce6@lipid-Gd-DOTA micelles (Ce6 2.4 μg/mL; Pdots 1.6 μg/mL) for 3h and subsequently irradiated under 670 nm laser. After treatment, the residual live cells were stained with live/dead viability/cytotoxicity kit by which the living cells show a green fluorescence, and the dead cells show a red fluorescence. As shown in Figure 4C, the HepG2 cells treated with Pdots/Ce6@lipid-Gd-DOTA micelles in the absence of laser irradiation or the HepG2 cells only treated with 670 nm laser irradiation without incubation with our lipid-micelles showed entire vivid green fluorescence, indicating low cytotoxicity of our Pdots/Ce6@lipid-Gd-DOTA micelles. However, several cells with red fluorescence could be clearly observed within the laser spot via the ROS-induced apoptosis (PDT) upon the 670 nm laser irradiation in Ce6-treated groups. Similar phenomenon could be also observed in the Pdots@lipid micelles-treated

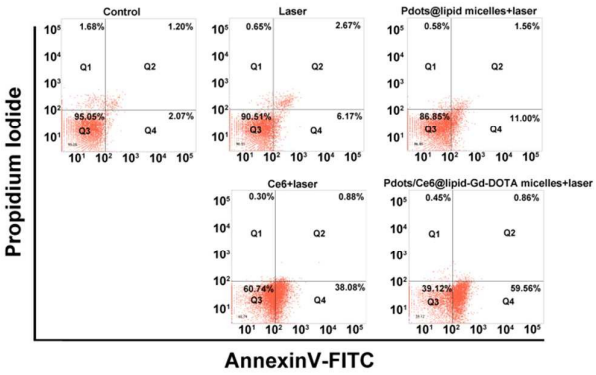

Figure 5. Apoptosis analysis of HepG2 cells incubated with Pdots/Ce6@lipid-Gd-DOTA micelles, free Ce6 or Pdots@lipid micelles followed by 670 nm laser irradiation, respectively. The cell apoptosis was determined by flow cytometry analysis using Annexin V-FITC and PI staining.

groups. Most significantly, almost no survived cells could be observed inside the laser spot in Pdots/Ce6@lipid-Gd-DOTA micelles-treated HepG2 cells in the presence of laser irradiation. These findings clearly demonstrated that our prepared Pdots/Ce6@lipid-Gd-DOTA micelles had excellent combined PDT/PTT effects against cancer cells.

To further analysis the apoptosis and necrosis of the treated cancer cells, flow cytometry analysis using Annexin-V-FITC / propidium iodide (PI) staining was performed. As shown in Figure 5, the stained cells were divided into four subgroups, and the viable group (Q3), the early apoptotic group (Q4), the late apoptotic / necrotic group (Q2) and the dead cells / debris group (Q1), respectively. As shown in Figure 5, the majority of cells were localized in the Q3 quadrant with more than 95.05% of the viable cells in the control group. Similarly, most of the cells without Pdots/Ce6@lipid-Gd-DOTA micelles treatment under 670 nm laser irradiation or with micelles treatment but in the absence of laser irradiation still maintained alive (above 90% of the viable cells). However, the percentage of viable cells was significantly decreased in the Pdots/Ce6@lipid-Gd-DOTA micelles treated groups under 670 nm laser irradiation (39.12% of the viable cells), comparing with the Ce6 treated groups (60.74% of the viable cells) or Pdots@lipid micelles treated group (80.58% of the viable cells), respectively. Accordingly, the percentage of apoptotic cells in Pdots/Ce6@lipid-Gd-DOTA micelles treated groups (60.42%) was much higher than the other two groups (38.96% in free Ce6 group and 12.56% in Pdots@lipid micelles group). These results clearly demonstrated the combined cell killing efficiency or dual-modal therapeutic effects of our Pdots/Ce6@lipid-Gd-DOTA micelles.

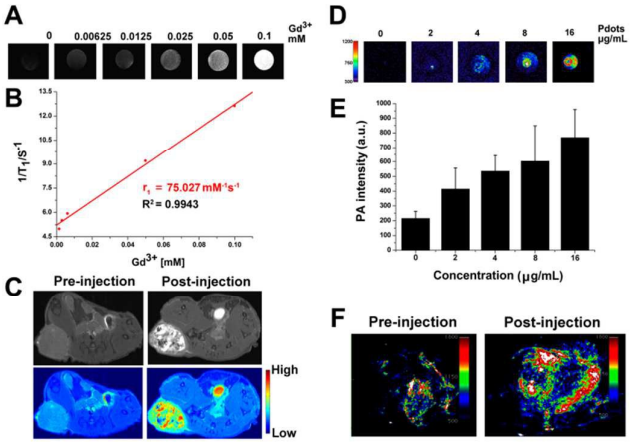

Figure 6. (A) T_1-weighted MR image of the Pdots/Ce6@lipid-Gd-DOTA micelles in aqueous solution at different Gd^{3+} concentrations. (B) The proton T_1 relaxation rate at various concentrations of Gd^{3+} in the Pdots/Ce6@lipid-Gd-DOTA micelles in a 9.4-T magnetic field. (C) Representative T_1-weighted MRI scans of mice pre- and post-injection of the Pdots/Ce6@lipid-Gd-DOTA micelles. (D) PA images and (E) PA intensity of aqueous dispersions contained different concentrarions of Pdots/Ce6@lipid-Gd-DOTA micelles. (F) PA images of tumor site at the time point of pre- and post-injection with Pdots/Ce6@lipid-Gd-DOTA micelles.

3.5. MR imaging and PA imaging of Pdots/Ce6@lipid-Gd-DOTA micelles

Contrast-enhanced MRI is one of the most powerful tool to provide the detailed anatomical information with high imaging quality for early detection of cancer and the assessment of therapeutic response [41]. Herein, we investigated the MRI contrast enhancement capability of our Pdots/Ce6@lipid-Gd-DOTA micelles on a 9.4 T MR imaging system (Siemens Magnetom Trio system). Tubes containing the various concentraition of the Pdots/Ce6@lipid-Gd-DOTA micelles were arrayed by increasing concentration, the water was placed as the control. As shown in Figure 6A, positive enhancement of the MRI in the Pdots/Ce6@lipid-Gd-DOTA micelles was observed compared to water, and the T_1-weighted MR images became brighter corresponding to the increase of the concentration of Pdots/Ce6@lipid-Gd-DOTA micelles. The T_1 relaxation time for each sample at 20°C was also analyzed, and the results indicated that the Pdots/Ce6@lipid-Gd-DOTA micelles shortened the T_1 relaxation time. Further analysis of the observed longitudinal rates revealed a linear dependence on the concentraton of dispersed Pdots/Ce6@lipid-Gd-DOTA micelles in all measurements (Figure 6B). The longitudinal coefficient relaxivity value, r1, which was determined from the slope of the plot of $1/T_1$ versus the sample concentration, was 75.027 $mM^{-1}s^{-1}$. To further verify the positive MRI signal enhancement capability of Pdots/Ce6@lipid-Gd-DOTA micelles in vivo, the prepared lipid-micelles were intratumorally injected into the nude mice bearing HepG2 tumor. As shown in Figure 6C, comparing to the pre-injection tumor section, the MRI signal was significantly enhanced after intratumoral injection of Pdots/Ce6@lipid-Gd-DOTA micelles, and showed a homogenous distribution of the contrast agents within the tumor. Moreover, the MRI signals of the tumor tissue were much stronger than surrounding normal tissue, indicating that the Pdots/Ce6@lipid-Gd-DOTA micelles have great potential for application in enhanced MR imaging of tumor.

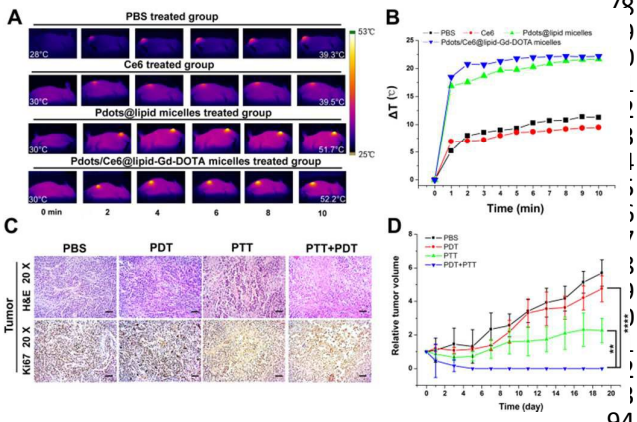

Figure 7. (A) Thermo-graphic images of tumor-bearing nude mice injected with PBS, free Ce6, Pdots@lipid micelles or Pdots/Ce6@lipid-Gd-DOTA micelles, which were exposed to 670nm laser irradiation (0.5 W/cm^2) at different time points, respectively. (B) Temperature changes of the tumor sites under 670nm laser irradiation at indicated treatment conditions. (C) Represectative images of H&E staining and immunohistochemical analysis from tumors after 24h of indicated treatments (Scale bar: 50 μm) (D)Tumor volumes of mice after different treatments as indicated. All data are presented as mean±SD (n = 4), and statistical analysis was performed with the two-tailed paired Student's T test, ** $p < 0.01$, **** $p < 0.0001$).

Photoacoustic imaging (PAI) is based on the detection of broadband ultrasonic waves generating from transient thermoelastic expansion after absorbing energy of the pulsed laser by photoacoustic contrast agents [43]. In this study, we investigated whether our Pdots/Ce6@lipid-Gd-DOTA micelles can be used as a photoacoustic contrast agent, inspired from the previous report that PCPDTBT nanohybrids had excellent photoacoustic effects [40]. As shown in Figure 6D and 6E, the PAI signal was increased along with the increasing of the concentration of Pdots/Ce6@lipid-Gd-DOTA micelles comparing to the control (water). To further verify the PAI signal enhancement capability in vivo, our Pdots/Ce6@lipid-Gd-DOTA micelles were intratumorally injected into the tumor site of HepG2 tumor bearing nude mice. As shown in Figure 6F, a much stronger PAI signal was clearly observed in the tumor region after intratumoral injection of Pdots/Ce6@lipid-Gd-DOTA micelles. These results clearly demonstrated that our lipid-micelles would be a promising condidate for in vivo MRI and PAI.

3.6. Synchronous photodynamic/photo-thermal therapy of tumor bearing mice in vivo

To evaluated the synergistic PDT / PTT effects of our Pdots/Ce6@lipid-Gd-DOTA micelles in vivo under single 670 nm laser irradiation, HepG2 tumor bearing mice model with initial tumor volumes of 130~170 mm^3 were chosen and randomly divided into 4 groups which were received various treatments as indicated (as mentioned in the Experimental Section). As shown in Figure 7A and 7B, the PTT effect of Pdots/Ce6@lipid-Gd-DOTA micelles was first studied by IR thermal camera. Rapid temperature rising at the tumor site, which was with intratumorally injected with the Pdots@lipid micelles (51.7°C) or Pdots/Ce6@lipid-Gd-DOTA micelles (52.2°C), was clearly observed under 670 nm laser irradiation. In contrast, only slight temperature change was observerd under the 670 nm laser irradiation at the tumor sites, which were injected with Ce6 or injected with PBS as control, respectively. To investigate the antitumor efficacy of the combined PDT / PTT treatment in vivo, H&E staining and immunohistochemical analysis of tumor tissues was performed after 24h of treatment, respectively. Tumor tissues from PBS treated mice were used as control. As shown in Figure 7C, no necrosis or obvious apotosis was observed in the tumor tissue slices of PBS treated group, and the tumor cells retained their normal morphotolgy with distinguishable membrane and nuclear structure. The tumors that received Ce6 treated group or Pdots@lipid micelles treated group showed a certain degree of tissue and cellular damage, due to the apoptosis of cancer cells induced by the PDT or PTT effect alone. It was notewhorthing that the combinded PDT / PTT treatment in Pdots/Ce6@lipid-Gd-DOTA micelles injected group showed significant cell destruction and extensive damaged areas, as indicated by the loss of tissue architectures and decreased general intensity of tissues. Meanwhile, the immunohistochemical (IHC) staining of tumor sections for antigen Ki67, which is significantly expressed in nucleus, was used to evaluate cell proliferation. As expected,

the Ki67 signal from the tumor cells that received the combined treatment of PDT and PTT in Pdots/Ce6@lipid-Gd-DOTA micelles treated mice was much weaker than other groups. Meanwhile, inspired by the efficient cell destruction of Pdots/Ce6@lipid-Gd-DOTA micelles treated mice, we conducted the tumor inhibition experiments by measuring the tumor volumes with a vernier caliper that continuously monitored for 19 days. As shown in Figure 7D, the mice experienced a rapid tumor growth in PBS treated group, indicating that PBS treatment followed by 670 nm laser irraditation had no influence on the tumor growth. In contrast, the Ce6 treated groups with 670nm laser irradiation showed delays in tumor growth but did not restrain the tumor growth, which might be the rapidly over-consumption of tissue oxygen that caused severe local hypoxia to cease the production of $^1O_2$ to influence on the PDT efficiency. Although the Pdots@lipid micelles treated group showed remarkable delays in tumor growth, it still could not restrain the tumor growth completely. However, it was noteworthy that Pdots/Ce6@lipid-Gd-DOTA micelles treated group exhibited much higher therapeutic efficiency and almost completely restrained the tumor growth over 19 days, compared with Ce6 treated or Pdots@lipid micelles treated group alone. The body weight of all groups were also recorded in our experiments after indicated treatments. As shown in Figure S7, no obvious weight loss was observed in Pdots@lipid micelles or Pdots/Ce6@lipid-Gd-DOTA micelles treated groups, comparing with the Ce6 or PBS treated group. These data clearly demonstrated that our Pdots/Ce6@lipid-Gd-DOTA micelles could serve as a highly effective PDT / PTT dual-modal therapeutic agent.

3.7. Long-term toxicity assessment of Pdots/Ce6@lipid-Gd-DOTA micelles

The potential toxicity of nanoparticle or nanodrug are greatly concerned throughout in vivo applications, and it has been proved that pathological change was an indicator for treatment induced toxicity. We next observed the pathological changes of major organs (heart, liver, spleen, lung, kidney) through the H&E staining at 0, 1, 8 and 20 day-post i.v. injection of Pdots/Ce6@lipid-Gd-DOTA micelles (100 μL per mouse, 0.1 mg/mL). PBS solution was set as control. As shown in Figure S8, there was also no noticeable tissue damaging in all major organs, comparing with the control groups. The above results showed that Pdots/Ce6@lipid-Gd-DOTA micelles were non-toxic at therapeutic dose (100 μL, 0.1 mg/mL).

Conclusions

In this work, we successfully developed the Pdots/Ce6@lipid-Gd-DOTA micelles as a multifuntiaonal theranostic agent for MR / PA dual-modal imaging and synchronous PDT / PTT treatment of liver cancers. The Pdots embedded into micelles exhitited strong PAI signal and high photothermal conversion ability and stability, and the Gd-DOTA modified on the outer showed a significant MRI enhancement ability, while the loaded Ce6 could achieve significant ROS generation under the same laser irradiation as PTT, respectively. The MR / PA dual-modal imaging signals of our micelles in tumor could be nicely observed both in vitro and in vivo. Antitumor study confirmed that our prepared Pdots/Ce6@lipid-Gd-DOTA micelles showed a significantly improved tumor killing efficacy, compared to the Pdots@lipid micelles or free Ce6 alone under 670 nm laser irradiation, which is demonstrated the synchronous PDT / PTT therapeutic effects of our micelles. Therefore, the prepared Pdots/Ce6@lipid-Gd-DOTA micelles might be used as a promising theranostic agent for MR / PA dual-modal imaging and synchronous PDT / PTT treatment of liver cancer.

Acknowledgements

This work was financially supported by the key clinical specialty discipline construction program of Fujian, P. R.C.; the specialized Science and Technology Key Project of Fujian Province (Grant No. 2013YZ0002-3); the Science and Technology Infrastructure Construction Program of Fujian Province (Grant No. 2014Y2005); the scientific innovation project of Fujian provincial Health and Family Planning Commission (Grant No. 2014-CX-32); the Scientific Foundation of Fuzhou Health Department (Grant No.2014-S-w18, Grant No.2014-S-w25); and the Backbone Talents Training Project of Fujian Health Department (Grant No. 2013-ZQN-ZD-29). We thank Wei Lin and Zhuanfang Li from Academy of Integrative Medicine, Fujian university of Traditional Chinese Medicine for technical assistance of the MR imaging.

Notes and references

1 V. Shanmugam, S. Selvakumar and C. S. Yeh, *Chem, Soc, Rev.*, 2014, **43**, 6254-6287.
2 J. T. Robinson, S. M. Tabakman, Y. Liang, H. Wang, H. S. Casalongue, D. Vinh and H. Dai, *J. Am. Chem. Soc*, 2011, **133**, 6825-6831.
3 P. Agostinis, K. Berg, K. A. Cengel, T. H. Foster, A. W. Girotti, S. O. Gollnick, S. M. Hahn, M. R. Hamblin, A. Juzeniene, D. Kessel, M. Korbelik, J. Moan, P. Mroz, D. Nowis, J. Piette, B. C. Wilson and J. Golab, *CA: Ca-Cancer, J, Clin.* 2011, **61**, 250-281.
4 L. Cheng, W. He, H. Gong, C. Wang, Q. Chen, Z. Cheng and Z. Liu, *Adv, Funct, Mat.* 2013, **23**, 5893-5902.
5 F. Li and K. Na, *Biomacromolecules,* 2011, **12**, 1724-1730.
6 W. S. Kuo, Y. T. Chang, K. C. Cho, K. C. Chiu, C. H. Lien, C. S. Yeh and S. J. Chen, *Biomaterials*, 2012, **33**, 3270-3278.
7 S. Sharifi, S. Behzadi, S. Laurent, M. L. Forrest, P. Stroeve and M. Mahmoudi, *Chem, Soc, Rev.* 2012, **41**, 2323-2343.
8 J. C. Bonner, *Exp, Rev, Respir, Med.* 2011, **5**, 779-787.
9 A. Albanese and W. C. Chan, *ACS Nano,* 2011, **5**, 5478-5489.
10 A. M. Alkilany, S. E. Lohse and C. J. Murphy, J., *Acc, Chem, Res.*2013, **46**, 650-661.
11 J. Ai, E. Biazar, M. Jafarpour, M. Montazeri, A. Majdi, S. Aminifard, M. Zafari, H. R. Akbari and H. G. Rad, *Int J Nanomed.* 2011, **6**, 1117-1127.
12 V. H. Fingar, *J, Clin, laser, Med, Sur.* 1996, **14**, 323-328.
13 D. E. Dolmans, D. Fukumura and R. K. Jain, *Nat, Rev, Cancer,* 2003, **3**, 380-387.
14 T. M. Busch, S. M. Hahn, S. M. Evans and C. J. Koch, *Cancer Res*, 2000, **60**, 2636-2642.
15 X. Song, C. Liang, H. Gong, Q. Chen, C. Wang and Z. Liu, *Small*, 2015.
16 D. Zhang, M. Wu, Y. Zeng, L. Wu, Q. Wang, X. Han, X. Liu and J. Liu, *ACS Appl. Mater. Interfaces.*2015, **7**, 8176-8187.
17 B. Jang, J.-Y. Park, C.-H. Tung, I.-H. Kim and Y. Choi, *ACS nano*, 2011, **5**, 1086-1094.
18 Y. Yong, L. Zhou, Z. Gu, L. Yan, G. Tian, X. Zheng, X. Liu, X. Zhang, J. Shi and W. Cong, *Nanoscale*, 2014, **6**, 10394-10403.
19 J. Lin, S. Wang, P. Huang, Z. Wang, S. Chen, G. Niu, W. Li, J. He, D. Cui and G. Lu, *ACS nano*, 2013, **7**, 5320-5329.

20 S. Wang, P. Huang, L. Nie, R. Xing, D. Liu, Z. Wang, J. Lin, S. Chen, G. Niu and G. Lu, *Adv, Mat.* 2013, **25**, 3055-3061.
21 X.-D. Zhang, D. Wu, X. Shen, P.-X. Liu, N. Yang, B. Zhao, H. Zhang, Y.-M. Sun, L.-A. Zhang and F.-Y. Fan, *Int, J, Nanomed.* 2011, **6**, 2071.
22 W. Cui, J. Li, Y. Zhang, H. Rong, W. Lu and L. Jiang, *Nanomed: Nanotechnol. Biology and Medicine*, 2012, **8**, 46-53.
23 S. Dhar, E. M. Reddy, A. Shiras, V. Pokharkar and B. e. L. e. V. Prasad, *Chem-A Euro, J.* 2008, **14**, 10244-10250.
24 M. O'brien, N. Wigler, M. Inbar, R. Rosso, E. Grischke, A. Santoro, R. Catane, D. Kieback, P. Tomczak and S. Ackland, *Ann, Oncol.* 2004, **15**, 440-449.
25 W. J. Gradishar, S. Tjulandin, N. Davidson, H. Shaw, N. Desai, P. Bhar, M. Hawkins and J. O'Shaughnessy, *J, Clin, Oncol,* 2005, **23**, 7794-7803.
26 N. Desai, V. Trieu, Z. Yao, L. Louie, S. Ci, A. Yang, C. Tao, T. De, B. Beals and D. Dykes, *Clin, Cancer Res.* 2006, **12**, 1317-1324.
27 C. F. van Nostrum, *Adv, Drug Deliver, Rev.* 2004, 56, 9-16.
28 M. Guo, H. Mao, Y. Li, A. Zhu, H. He, H. Yang, Y. Wang, X. Tian, C. Ge and Q. Peng, *Biomaterials,* 2014, **35**, 4656-4666.
29 L. Gibot, A. Lemelle, U. Till, B. a. Moukarzel, A.-F. o. Mingotaud, V. r. Pimienta, P. Saint-Aguet, M.-P. Rols, M. Gaucher and F. d. r. Violleau, *Biomacromolecules,* 2014, **15**, 1443-1455.
30 Z. Wan, H. Mao, M. Guo, Y. Li, A. Zhu, H. Yang, H. He, J. Shen, L. Zhou and Z. Jiang, *Theranostics*, 2014, 4, 399.
31 W.-H. Jian, T.-W. Yu, C.-J. Chen, W.-C. Huang, H.-C. Chiu and W.-H. Chiang, *Langmuir*, 2015.
32 A. Jackson, J. P. O'Connor, G. J. Parker and G. C. Jayson, *Clin, Cancer, Res.* 2007, **13**, 3449-3459.
33 A. De Schepper, L. De Beuckeleer, J. Vandevenne and J. Somville, *Euro, Radio.* 2000, **10**, 213-223.
34 L.-S. Bouchard, M. S. Anwar, G. L. Liu, B. Hann, Z. H. Xie, J. W. Gray, X. Wang, A. Pines and F. F. Chen, *Proc. Nat. Acad. Sci*, 2009, **106**, 4085-4089.
35 B. Morgan, A. L. Thomas, J. Drevs, J. Hennig, M. Buchert, A. Jivan, M. A. Horsfield, K. Mross, H. A. Ball and L. Lee, *J, Clin, Oncol.* 2003, **21**, 3955-3964.
36 X. Liang, Y. Li, X. Li, L. Jing, Z. Deng, X. Yue, C. Li and Z. Dai, *Adv. Funct. Mater.* 2015, **25**, 1451-1462.
37 L. Nie and X. Chen, *Chem, Soc, Rev.* 2014, 43, 7132-7170.
38 S. Sreejith, J. Joseph, M. Lin, N. V. Menon, P. Borah, H. J. Ng, Y. X. Loong, Y. Kang, S. W.-K. Yu and Y. Zhao, *ACS Nano,* 2015.
39 D. Mühlbacher, M. Scharber, M. Morana, Z. Zhu, D. Waller, R. Gaudiana and C. Brabec, *Adv. Mater.* 2006, **18**, 2884-2889.
40 K. Pu, A. J. Shuhendler, J. V. Jokerst, J. Mei, S. S. Gambhir, Z. Bao and J. Rao, *Nat. nanotech.* 2014, **9**, 233-239.
41 G. Feng, K. Li, J. Liu, D. Ding and B. Liu, *Small*, 2014, **10**, 1212-1219.
42 Y. Zeng, D. Zhang, M. Wu, Y. Liu, X. Zhang, L. Li, Z. Li, X. Han, X. Wei and X. Liu, *ACS Appl. Mater. Interfaces.* 2014, **6**, 14266-14277.
43 K. Li and B. Liu, *Chem, Soc, Rev.* 2014, **43**, 6570-6597.

Lipid-micelles packaged with semiconducting polymer dots as simultaneous MRI / photoacoustic imaging and photodynamic /photothermal dual-modal therapeutic agents for liver cancer

Da Zhang, [†,‡] Ming Wu, [†,‡] Yongyi Zeng, [†,‡,§] Naishun Liao, [†,‡] Zhixiong Cai, [†,‡] Gang Liu, [|]

Xiaolong Liu[†,‡]*, Jingfeng Liu[†,‡,§]*

*Corresponding Author (correspondence should be address to Xiaolong Liu and Jingfeng Liu), E-mail addresses: xiaoloong.liu@gmail.com, drjingfeng@126.com

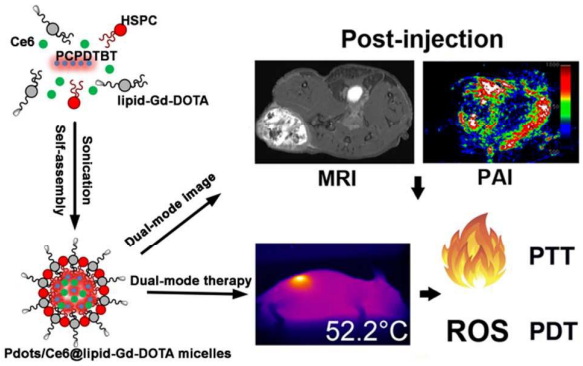

Semiconducting polymer dots micelles for MRI/photoacoustic imaging and single laser induced PDT / PTT therapy.